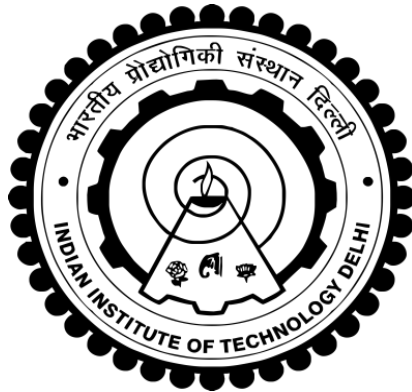


# **CONTROL OF SOLAR PV-BES-WIND BASED STANDALONE AND GRID CONNECTED AC MICROGRIDS WITH SYNCHRONIZATION**

**GAURAV MODI**



**DEPARTMENT OF ELECTRICAL ENGINEERING  
INDIAN INSTITUTE OF TECHNOLOGY DELHI  
HAUZ KHAS, NEW DELHI-110016, INDIA**

**AUGUST 2024**

© Indian Institute of Technology Delhi (IITD), New Delhi, 2024

**CONTROL OF SOLAR PV-BES-WIND BASED  
STANDALONE AND GRID CONNECTED AC  
MICROGRIDS WITH SYNCHRONIZATION**

By

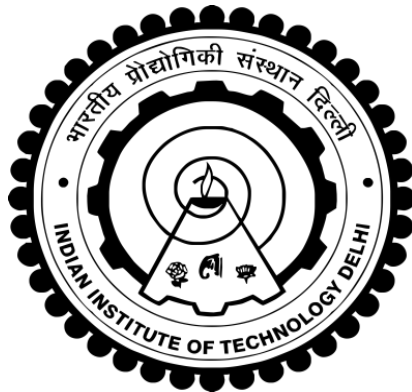
**Gaurav Modi**

**Electrical Engineering Department**

*Submitted*

*in fulfilment of the requirement of the degree of Doctor of Philosophy*

**to the**



**INDIAN INSTITUTE OF TECHNOLOGY DELHI**

**AUGUST 2024**

## **CERTIFICATE**

It is certified that the thesis entitled “**Control of Solar PV-BES-Wind Based Standalone and Grid Connected AC Microgrids with Synchronization,**” being submitted by **Mr. Gaurav Modi** for award of the degree of **Doctor of Philosophy** in the Department of Electrical Engineering, Indian Institute of Technology Delhi, is a record of the student work carried out by him under my supervision and guidance. The matter embodied in this thesis has not been submitted for award of any other degree or diploma.

**Dated:**

**(Prof. Bhim Singh)**  
**Electrical Engineering Department**  
**Indian Institute of Technology Delhi**  
**Hauz Khas, New Delhi-110016, India**

## ACKNOWLEDGEMENTS

I wish to express my deepest gratitude and indebtedness to **Prof. Bhim Singh** for his unwavering guidance and supervision throughout my Ph.D. journey. Working under his mentorship has been an enriching experience, providing me with profound insights into the realm of research. Determination, dedication, innovativeness, resourcefulness and discipline of **Prof. Bhim Singh** have served as a constant source of inspiration, propelling me to successfully complete this work. His consistent encouragement, meticulous oversight, and commitment to excellence have continuously motivated me to strive for improvement and harness my full potential. Under his tutelage and blessing, I have not only gained invaluable research experiences but also acquired skills that will benefit me throughout my life.

I extend my heartfelt thanks and deep gratitude to **Prof. G. Bhuvanewari, Prof. Nilanjan Senroy, Prof. Anandarup Das, Prof. Ashu Verma, Dr. Ramkrishan Maheshwari**, and all SRC members for their invaluable guidance and unwavering support during my research work.

I also express my sincere appreciation to **Prof. Bhim Singh, Prof. B. P. Singh, Prof. Sukumar Mishra**, and **Dr. Ramkrishan Maheshwari** for their invaluable insights during my coursework, laying a strong foundation for my research. I am thankful to the **Indian Institute of Technology Delhi** for providing me with the necessary research facilities.

Special thanks are due to **Prof. Bhim Singh** and **Prof. M. Veerachary**, as Prof. in-charge of PG Machine Lab, generously providing me with facilities to conduct experimental work at the PG Machine Lab. Additionally, I am grateful to **Prof. Chandan Chakraborty, Prof. Jianzhong Wu, and Prof. Nick Jenkins**, for their valuable support and guidance during collaborative work under “**Indo-UK, project UKICERI (UK-INDIA Clean Energy Research Institute)**” project.

I extend my gratitude to Sh. Srichand, Sh. Puran Singh, Sh. Jagbir Singh, Sh. Amit Kumar, and Sh. Jitendra of PG Machines Lab, UG Machines Lab and Power Electronics Lab., Indian Institute of Technology Delhi for their assistance and provision of facilities.

I would like to thank all my seniors, Dr. Ikhlq Hussain, Dr. Sachin Devassy, Dr. Aniket Anand, Dr. Nishant Kumar, Dr. Khusro Khan, Dr. Shadab Murshid, Dr. Anshul Varshney, Dr. Sreejith R, Dr. Saurabh Shukla, Dr. Shatakshi Jha, Dr. Shailendra Kumar Dwivedi, Dr. Piyush Kant, Dr. Seema Kewat, Dr. Radha Khushwaha, Dr. Priyank Mukeshkumar Shah, Dr. VL Srinivas, Dr. Anjeet Kumar Verma, Dr. Subarni Pradhan, Dr. Anjaneer Kumar Mishra, Dr. Deepu Vijay M,

Dr. Utkarsh Sharma, Mr. Debasish Mishra, Mr. P. Sambasivaiah, Dr. Pavitra Shukl, Dr. Farheen Chishti, Dr. Rohini Sharma, Dr. Mohd. Kashif, Ms. Hina Parveen, Mr. Aryadip Sen, and Mr. Yalavarthi Amarnath, who have constantly helped me on all technical and non-technical issues.

My sincere thanks are due to for cooperation and informal support Dr. Shailendra Kumar Dwivedi, Dr. Shadab Murshid, Dr. Anshul Varshney, Dr. Piyush Kant, Dr. Seema Kewat, Dr. Subarni Pradhan, Dr. Utkarsh Sharma, Dr. Farheen Chishti, Dr. Rohini Sharma, Ms. Hina Parveen, Mr. Aryadip Sen, and Mr. Yalavarthi Amarnath, in pursuing this research work.

Special thanks to Dr. Souvik Das, Dr. Jitendra Gupta, Mr. Utsav Sharma, Mrs. Shalvi Tyagi, Mr. Syed Bilal Qaiser Naqvi, Mr. Sudip Bhattacharyya, Mr. Sandeep Kumar Sahoo, Mrs. Yashi Singh, Mr. Subhadip Chakraborty and all other colleges for their valuable aid and cooperation.

Moreover, I would like to thank, Dr. Vivek Narayanan, Mr. Saran Chaurasiya, Mr. Sayandev Ghosh, Mr. Suri Rama Naga Praneeth, Mr. Priyvrat Vats, Mr. Rahul Kumar, Mr. Sharankumar Shastri, Mr. Deepak Saw, Mr. Shivam Kumar Yadav, Mrs. Kousalya V, Ms. Sanjenbam Chandrakala Devi, Mr. Saurabh Mishra, Mr. Mohammad Junaid, Mr. Muhammad Zarkab Farqooi, Mrs. Kripa Tiwari, Mr. Rohit Kumar, Mr. Vipin Kumar Singh, Mr. Arjun Kumar, Mr. Biswajit Saha, Ms. Farha Siddique, Mr. Sumit Kumar, Mr. Gaurav Kumar, Mr. Himansu Sahoo, Mr. Adnan Farooq Khan, Mr. Chetan Shashank Matwankar, Ms. Smita Mohanty, and all PG Machines lab group for their valuable support.

Moreover, I would like to thank Department of Science and Technology (DST), Govt. of India for funding this research work under the fund for improvement of S&T infrastructure in higher educational institutions (FIST), UKICERI (RP03391), Clean Energy (RP03195), UI-ASSIST (RP03443), SERIII, J C Bose Fellowship (RP03128) and SERB NSC Fellowship.

I am deeply indebted to my parents, Mrs. Madhu Modi and Mr. Mukesh Modi, for their unwavering support and encouragement. Special thanks to my elder sisters, Swati Agrawal and Kamini Kansal, and friends, Mrs. Aarti Bandil and Mr. Ashish Kulshrestha, for their continuous support and belief in my abilities.

Finally, I express my gratitude to the Almighty for blessing me with the strength, wisdom, and determination to reach this academic milestone. I pray for their continued guidance and blessings in all my future endeavors.

**Dated:**

**Gaurav Modi**

## ABSTRACT

This thesis presents a comprehensive approach to controlling solar PV-BES-wind-based standalone and grid-connected AC microgrids with synchronization. Throughout this research, various configurations pertaining to solar PV-based microgrids are investigated, taking into account the specific needs of low and medium-income consumers in both urban and rural settings. Furthermore, the exploration of microgrid configurations is expanded to include solar PV-BES-wind-based systems, leading to the development of a novel structure that optimizes the benefits of existing frameworks in a cost-effective manner. Additionally, the thesis delves into the feasibility of employing synchronous reluctance generators (SyRGs) as a cost-effective alternative to PMSGs for small-scale WES, further enhancing the affordability and accessibility of renewable energy solutions.

To confront emerging power quality challenges stemming from nonlinear loads, this thesis devises innovative control strategies. These strategies leverage the architecture of traditional control algorithms, providing effective solutions with ease of implementation. In response to synchronization challenges, the thesis introduces improved filter algorithms that demonstrate enhanced responsiveness while maintaining low computational complexity. Consequently, these advancements address the limitations inherent in existing synchronization algorithms.

Furthermore, power management schemes are meticulously crafted to align with specific consumer and application needs, considering practical constraints of system. These schemes encompass a range of aspects, including providing grid support by ensuring that any increase in PCC voltage remains within predefined standards.

In the context of DG-based standalone microgrids, this thesis proposes innovative control strategies based on multimode operation to minimize the utilization of DG sets. These strategies entail the operation of microgrids in both standalone mode and DG-connected mode, with the latter being activated exclusively during emergencies. Upon the microgrid's ability to fulfil load demand through RES and BES, the DG-connected mode is promptly deactivated. To address technical challenges associated with seamlessly transitioning microgrid operation between different modes in multimode operation-based grid-connected microgrids, robust and straightforward solutions are developed. Furthermore, these solutions are extended to DG-based standalone microgrids to facilitate seamless transitions between standalone operational mode and DG-connected mode.

To validate the performance of the proposed microgrid configurations and engineered control strategies, simulations are conducted using MATLAB/Simulink in MATLAB 2017B software.

The response of the microgrids and their controls is thoroughly examined in this virtual environment. Subsequently, hardware implementation and real-time analysis are employed to further investigate the performance of the configured microgrids and their control strategies, aiming to validate the simulated results. The obtained findings conclusively demonstrate the successful achievement of the defined objectives outlined in this thesis work.

## सार

इस शोध प्रबंध में सौर फोटोवोल्टाइक, बैटरी ऊर्जा भंडारण और पवन-आधारित स्टैंडअलोन और ग्रिड से जुड़े एसी माइक्रोग्रिड्स के नियंत्रण के लिए एक व्यापक दृष्टिकोण प्रस्तुत किया गया है। इस शोध के दौरान, शहरी और ग्रामीण दोनों क्षेत्रों में निम्न और मध्यम आय वाले उपभोक्ताओं की विशेष आवश्यकताओं को ध्यान में रखते हुए सौर पीवी-आधारित माइक्रोग्रिड्स के विभिन्न कॉन्फिगरेशन की जांच की गई है। इसके अलावा, माइक्रोग्रिड कॉन्फिगरेशन की खोज को सौर पीवी-बैटरी ऊर्जा भंडारण-पवन-आधारित प्रणालियों तक विस्तारित किया गया है, जिसके परिणामस्वरूप एक नए ढांचे का विकास हुआ है जो मौजूदा फ्रेमवर्क के लाभों को एक लागत-प्रभावी तरीके से अनुकूलित करता है। इसके अतिरिक्त, इस शोध प्रबंध में छोटे पैमाने के पवन ऊर्जा प्रणाली के लिए स्थायी चुंबक सिंक्रोनस जनरेटर के लागत-प्रभावी विकल्प के रूप में सिंक्रोनस रीलक्टेस जनरेटर के उपयोग की व्यवहार्यता की जांच की गई है, जिससे नवीकरणीय ऊर्जा समाधानों की पहुंच और अधिक किफायती बन सके।

गैर-रैखिक लोड से उत्पन्न हो रही उभरती हुई बिजली की गुणवत्ता की चुनौतियों का सामना करने के लिए, इस शोध प्रबंध में नवाचारपूर्ण नियंत्रण रणनीतियाँ तैयार की गई हैं। ये रणनीतियाँ पारंपरिक नियंत्रण एल्गोरिदम की संरचना का लाभ उठाती हैं, जिससे उन्हें प्रभावी ढंग से लागू करना आसान होता है। सिंक्रोनाइज़ेशन चुनौतियों के प्रति प्रतिक्रिया में, शोध प्रबंध में बेहतर फिल्टर एल्गोरिदम पेश किए गए हैं जो कम कम्प्यूटेशनल जटिलता बनाए रखते हुए बेहतर प्रतिक्रिया क्षमता प्रदर्शित करते हैं। नतीजतन, ये प्रगति मौजूदा सिंक्रोनाइज़ेशन एल्गोरिदम की अंतर्निहित सीमाओं को संबोधित करती है।

इसके अलावा, उपभोक्ता और अनुप्रयोग की विशिष्ट आवश्यकताओं के अनुरूप पावर प्रबंधन योजनाएं सावधानीपूर्वक तैयार की जाती हैं, जो सिस्टम की व्यावहारिक बाधाओं को ध्यान में रखते हुए होती हैं। इन योजनाओं में पॉइंट ऑफ़ कॉमन कप्लिंग वोल्टेज में किसी भी वृद्धि को पूर्वनिर्धारित मानकों के भीतर बनाए रखते हुए ग्रिड समर्थन प्रदान करना शामिल है।

डीजल जनरेटर आधारित स्टैंडअलोन माइक्रोग्रिड्स के संदर्भ में, इस शोध प्रबंध में मल्टीमोड ऑपरेशन के आधार पर डीजल जनरेटरों के उपयोग को कम करने के लिए नवाचारी नियंत्रण रणनीतियों का प्रस्ताव किया गया है। इन रणनीतियों में माइक्रोग्रिड्स को स्टैंडअलोन मोड और डीजल जनरेटर कनेक्टेड मोड दोनों में संचालित करना शामिल है, जिसमें बाद वाला केवल आपातकालीन स्थितियों में सक्रिय होता है। जैसे ही माइक्रोग्रिड नवीकरणीय ऊर्जा स्रोतों और बैटरी ऊर्जा भंडारण के माध्यम से लोड मांग को पूरा करने में सक्षम होता है, डीजल जनरेटर कनेक्टेड मोड को तुरंत निष्क्रिय कर दिया जाता है। मल्टीमोड ऑपरेशन-आधारित ग्रिड से जुड़े माइक्रोग्रिड्स में विभिन्न मोड के बीच सुगम संक्रमण के साथ संबंधित

तकनीकी चुनौतियों को संबोधित करने के लिए, मजबूत और सरल समाधान विकसित किए गए हैं। इसके अलावा, ये समाधान डीजल जनरेटर आधारित स्टैंडअलोन माइक्रोग्रिड्स तक विस्तारित किए गए हैं ताकि स्टैंडअलोन ऑपरेशनल मोड और डीजल जनरेटर कनेक्टेड मोड के बीच सुगम संक्रमण की सुविधा हो सके।

प्रस्तावित माइक्रोग्रिड कॉन्फिगरेशन और डिज़ाइन किए गए नियंत्रण रणनीतियों के प्रदर्शन को मान्य करने के लिए, मैटलैब 2017बी सॉफ्टवेयर में MATLAB/Simulink का उपयोग करके सिमुलेशन किए गए हैं। इस आभासी वातावरण में माइक्रोग्रिड्स और उनके नियंत्रण की प्रतिक्रिया की पूरी तरह से जांच की गई है। इसके बाद, हार्डवेयर कार्यान्वयन और वास्तविक समय विश्लेषण का उपयोग करके कॉन्फिगर किए गए माइक्रोग्रिड्स और उनकी नियंत्रण रणनीतियों के प्रदर्शन की आगे की जांच की गई है, जिसका उद्देश्य सिमुलेशन परिणामों को मान्य करना है। प्राप्त निष्कर्ष स्पष्ट रूप से इस शोध कार्य में उल्लिखित परिभाषित उद्देश्यों की सफल उपलब्धि को प्रदर्शित करते हैं।

# TABLE OF CONTENTS

	<b>Page No.</b>
Certificate	i
Acknowledgements	ii
Abstract	iv
Table of Contents	viii
List of Figures	xxi
List of Tables	xxxv
List of Abbreviations	xxxvi
List of Symbols	xxxviii
<b>CHAPTER-I INTRODUCTION</b>	<b>1-12</b>
1.1 General	1
1.2 State of Art on SPV-BES-Wind Based AC Microgrid	3
1.3 Objectives and Scope of Work	7
1.4 Organization of Thesis	11
<b>CHAPTER -II LITERATURE REVIEW</b>	<b>13-28</b>
2.1 General	13
2.2 Review of Solar Photovoltaic System (SPVS)	13
2.2.1 MPPT Algorithm for SPVS	15
2.3 Review of Wind Energy System (WES)	16
2.3.1 MPPT Algorithm for WES	17
2.4 Review of Integration of BES with RES Based AC Microgrid	18
2.5 Review of SPV-Wind-BES Based AC Microgrid	19
2.6 Review of Control Strategies for Grid Side Converter (GSC) of AC Microgrid	20
2.6.1 Review of Control Strategies for VCA Based Control Architecture of GSC	21
2.6.2 Review of Control Strategies for CCA Based Control Architecture of GSC	22
2.7 Review of Synchronization Algorithms for AC Microgrid	23
2.8 Review of Multi-Functional Capabilities of AC Microgrid	25
2.9 Review of Multimode Operation of AC Microgrid	26
2.10 Identified Research Areas	27
2.11 Conclusions	28
<b>CHAPTER – III CONTROL OF THREE-PHASE SPV SYSTEM WITH AND WITHOUT BES WITH SYNCHRONIZATION</b>	<b>29-107</b>
3.1 General	29
3.2 Configurations of Three Phase SPV Systems	29
3.2.1 Three Phase Single Stage SPVS Without BES	30

3.2.2	Three Phase Two Stage SPVS Without BES	31
3.2.3	Three Phase Two Stage SPVS with Direct Integration of BES at DC Link	31
3.2.4	Three Phase Single Stage SPVS with Integration of BES at DC Link by a BDDC	32
3.2.5	Three Phase Two Stage SPVS with Integration of BES at DC Link by a BDDC	32
3.3	Design of Three Phase SPV Systems	33
3.3.1	Selection of PGSC's Rating and its Various Elements	33
3.3.2	Selection of SPV Array Parameters	34
3.3.2.1	Selection of Single-Stage SPV Array Parameters	34
3.3.2.2	Selection of Two-Stage SPV Array Parameters	35
3.3.3	Selection of BES Parameters	35
3.3.3.1	Selection of BES Parameters for Its Direct Integration at DC Link	35
3.3.3.2	Selection of BES Parameters for Its Integration at DC Link by a BDDC	36
3.3.4	Selection of Interfacing Inductor, Ripple Filter, and Inductances of BTC and BDDC	36
3.3.4.1	Design of Interfacing Inductor	36
3.3.4.2	Design of Ripple Filter	37
3.3.4.3	Design of Inductances of BTC and BDDC	37
3.4	Control Approaches of Three Phase SPV Systems	37
3.4.1	Procedure for Operating Modes Selection	38
3.4.2	Estimation of AC Grid Voltage Parameters	40
3.4.3	Control of Three Phase Single Stage SPVS Without BES	45
3.4.3.1	Control of Three Phase Single Stage SPVS Without BES During Grid Connected Mode	45
3.4.3.2	Control of Three Phase Single Stage SPVS Without BES During Standalone Mode	48
3.4.4	Control of Three Phase Two Stage SPVS Without BES	49
3.4.4.1	Control of Three Phase Two Stage SPVS Without BES During Grid Connected Mode	50
3.4.4.2	Control of Three Phase Two Stage SPVS Without BES During Standalone Mode	50
3.4.5	Control of Three Phase Two Stage SPVS with Direct Integration of BES at DC Link	51
3.4.5.1	Control of Three Phase Two Stage SPVS with Direct Integration of BES at DC Link During Grid Connected Mode	51
3.4.5.2	Control of Three Phase Two Stage SPVS with Direct Integration of BES at DC Link During Standalone Mode	52

3.4.6	Control of Three Phase Single Stage SPVS with Integration of BES at DC Link by a BDDC	54
3.4.6.1	Control of Three Phase Single Stage SPVS with Integration of BES at DC Link by a BDDC During Grid Connected Mode	54
3.4.6.2	Control of Three Phase Single Stage SPVS with Integration of BES at DC Link by a BDDC During Standalone Mode	56
3.4.7	Control of Three Phase Two Stage SPVS with Integration of BES at DC Link by a BDDC	57
3.4.7.1	Control of Three Phase Two Stage SPVS with Integration of BES at DC Link by a BDDC During Grid Connected Mode	57
3.4.7.2	Control of Three Phase Two Stage SPVS with Integration of BES at DC Link by a BDDC During Standalone Mode	61
3.5	MATLAB Based Modelling of Three Phase SPV System	61
3.5.1	MATLAB Model of Three Phase Single Stage SPVS Without BES	62
3.5.2	MATLAB Model of Three Phase Two Stage SPVS Without BES	62
3.5.3	MATLAB Model of Three Phase Two Stage SPVS with Direct Integration of BES at DC Link	63
3.5.4	MATLAB Model of Three Phase Single Stage SPVS with Integration of BES at DC Link by a BDDC	63
3.5.5	MATLAB Model of Three Phase Two Stage SPVS with Integration of BES at DC Link by a BDDC	64
3.6	Hardware Implementation of Three Phase SPV System	65
3.6.1	Specification of DS1103 PPC Controller Board	66
3.6.2	Interfacing Circuit for Hall Effect Based Voltage and Current Sensors	67
3.6.3	Interfacing Circuit for Opto-Coupler or Gate Driver	67
3.7	Results and Discussion	68
3.7.1	Performance of Three Phase Single Stage SPVS Without BES	68
3.7.1.1	Simulated Performance of Three Phase Single Stage SPVS Without BES During Grid Connected Operational Mode	68
3.7.1.2	Simulated Performance of Three Phase Single Stage SPVS Without BES During Standalone Operational Mode	70

3.7.1.3	Simulated Performance of Three Phase Single Stage SPVS Without BES During Change in Operational Mode	72
3.7.1.4	Experimental Performance of Three Phase Single Stage SPVS Without BES During Grid Connected Operational Mode	72
3.7.1.5	Experimental Performance of Three Phase Single Stage SPVS Without BES During Standalone Operational Mode	76
3.7.1.6	Experimental Performance of Three Phase Single Stage SPVS Without BES During Change in Operational Mode	76
3.7.2	Performance of Three Phase Two Stage SPVS Without BES	78
3.7.2.1	Simulated Performance of Three Phase Two Stage SPVS Without BES During Grid Connected Operational Mode	79
3.7.2.2	Simulated Performance of Three Phase Two Stage SPVS Without BES During Change in Operational Mode	80
3.7.2.3	Experimental Performance of Three Phase Two Stage SPVS Without BES During Grid Connected Operational Mode	80
3.7.2.4	Experimental Performance of Three Phase Two Stage SPVS Without BES During Standalone Operational Mode	81
3.7.2.5	Experimental Performance of Three Phase Two Stage SPVS Without BES During Change in Operational Mode from Standalone to Grid Connected	83
3.7.3	Performance of Two Stage SPVS with Direct Integration of BES at DC Link	83
3.7.3.1	Simulated Performance of Three Phase Two Stage SPVS with Direct Integration of BES at DC Link During Grid-Tied Operational Mode	84
3.7.3.2	Simulated Performance of Three Phase Two Stage SPVS with Direct Integration of BES at DC Link During Standalone Operational Mode	86
3.7.3.3	Simulated Performance of Three Phase Two Stage SPVS with Direct Integration of BES at DC Link During Change in Operational Mode	86
3.7.3.4	Experimental Performance of Three Phase Two Stage SPVS with Direct Integration of BES at DC Link During Grid Connected Operational Mode	87

3.7.3.5	Experimental Performance of Three Phase Two Stage SPVS with Direct Integration of BES at DC Link During Change in Operational Mode	90
3.7.4	Performance of Three Phase Single Stage SPVS with Integration of BES at DC Link by a BDDC	91
3.7.4.1	Simulated Performance of Three Phase Single Stage SPVS with Integration of BES at DC Link by a BDDC During Grid-Tied Operational Mode	91
3.7.4.2	Simulated Performance of Three Phase Single Stage SPVS with Integration of BES at DC Link by a BDDC During Change in Operational Mode	94
3.7.4.3	Experimental Performance of Three Phase Single Stage SPVS with Integration of BES at DC Link by a BDDC During Grid Connected Operational Mode	95
3.7.4.4	Experimental Performance of Three Phase Single Stage SPVS with Integration of BES at DC Link by a BDDC During Change in Operational Mode	96
3.7.5	Performance of Three Phase Two Stage SPVS with Integration of BES at DC Link by a BDDC	97
3.7.5.1	Simulated Performance of Three Phase Two Stage SPVS with Integration of BES at DC Link by a BDDC During Grid Connected Operational Mode	98
3.7.5.2	Simulated Performance of Three Phase Two Stage SPVS with Integration of BES at DC Link by a BDDC During Change in Operational Mode	100
3.7.5.3	Experimental Performance of Three Phase Two Stage SPVS with Integration of BES at DC Link by a BDDC	102
3.8	Conclusions	106
<b>CHAPTER-IV</b>	<b>CONTROL OF THREE-PHASE FOUR-WIRE SPV BASED GRID INTERACTIVE SYSTEM WITH AND WITHOUT BES</b>	<b>108-152</b>
4.1	General	108
4.2	Configurations of Three-Phase Four-Wire SPV Systems	108
4.2.1	Three-Phase Four-Wire Single Stage SPV System Without BES	109
4.2.2	Three-Phase Four-Wire Two Stage SPV System Without BES	109
4.2.3	Three-Phase Four-Wire Two-Stage SPV System with Direct Integration of BES at DC Link	110

4.2.4	Three-Phase Four-Wire Single-Stage SPV System with Integration of BES at DC Link by a BDDC	111
4.2.5	Three-Phase Four-Wire Two-Stage SPV System with Integration of BES at DC Link by a BDDC	111
4.3	Design of Three-Phase Four-Wire SPV Systems	112
4.3.1	Selection of Interfacing Inductor of 4 <sup>th</sup> Leg (PGSC Neutral Leg)	112
4.4	Control Approaches of Three-Phase Four-Wire SPV Systems	112
4.4.1	Structure of Fractional Least Mean Square (F-LMS) Algorithm	113
4.4.2	Control of Three-Phase Four-Wire Single Stage SPV System Without BES	115
4.4.3	Control of Three-Phase Four-Wire Two Stage SPV System Without BES	118
4.4.4	Control of Three-Phase Four-Wire Two-Stage SPV System with Direct Integration of BES at DC Link	121
4.4.5	Control of Three-Phase Four-Wire Single-Stage SPV System with Integration of BES at DC Link by a BDDC	122
4.4.6	Control of Three-Phase Four-Wire Two-Stage SPV System with Integration of BES at DC Link by a BDDC	123
4.5	MATLAB Based Modelling of Three Phase Four-Wire SPV Systems	123
4.6	Hardware Implementation of Three Phase Four-Wire SPV Systems	124
4.7	Results and Discussion	127
4.7.1	Performance of Three-Phase Four-Wire Single Stage SPV System Without BES	127
4.7.1.1	Simulated Performance of Three Phase Four-Wire Single Stage SPV System Without BES	127
4.7.1.2	Experimental Performance of Three Phase Four-Wire Single Stage SPV System Without BES	129
4.7.2	Performance of Three-Phase Four-Wire Two Stage SPV System Without BES	134
4.7.2.1	Simulated Performance of Three-Phase Four-Wire Two Stage SPV System Without BES	134
4.7.2.2	Experimental Performance of Three-Phase Four-Wire Two Stage SPV System Without BES	136
4.7.3	Performance of Three-Phase Four-Wire Two-Stage SPV System with Direct Integration of BES at DC Link	139
4.7.3.1	Simulated Performance of Three-Phase Four-Wire Two Stage SPV System with Direct Integration of BES	139
4.7.3.2	Experimental Performance of Three-Phase Four-Wire Two Stage SPV System with Direct Integration of BES	140

4.7.4	Performance of Three-Phase Four-Wire Single Stage SPV System with Integration of BES at DC Link by a BDDC	143
4.7.4.1	Simulated Performance of Three Phase Four-Wire Single Stage SPV System with Integration of BES at DC Link by a BDDC	144
4.7.4.2	Experimental Performance of Three Phase Four-Wire Single Stage SPV System with Integration of BES at DC Link by a BDDC	144
4.7.5	Performance of Three-Phase Four-Wire Two Stage SPV System with Integration of BES at DC Link by a BDDC	147
4.7.5.1	Simulated Performance of Three Phase Four-Wire Two Stage SPV System with Integration of BES at DC Link by a BDDC	147
4.7.5.2	Experimental Performance of Three Phase Four-Wire Two Stage SPV System with Integration of BES at DC Link by a BDDC	148
4.8	Conclusions	151
<b>CHAPTER-V</b>	<b>CONTROL OF SPV-BES-WIND-BASED THREE-PHASE STANDALONE MICROGRID</b>	<b>153-195</b>
5.1	General	153
5.2	Configurations of SPV-BES-WIND-Based Three-Phase Standalone Microgrids	154
5.2.1	Three-Phase Two-Stage SPV-BES-Wind Based Standalone Microgrid	154
5.2.2	Three-Phase Single-Stage SPV-BES-Wind Based Standalone Microgrid with BDDC	155
5.2.3	Three-Phase Two-Stage SPV-BES-Wind Based Standalone Microgrid with BDDC	156
5.3	Design of SPV-BES-Wind-Based Three-Phase Standalone Microgrids	156
5.3.1	Design Principle of WES	157
5.3.1.1	Design of Wind Turbine Generator Assembly (WTGA)	157
5.3.1.2	Selection of SyRG Based Wind Generator (WG) Rating	158
5.3.1.3	Selection of WGSC's Rating and its Various Elements	158
5.3.1.4	Selection of MSC Rating	159
5.3.1.5	Selection of Interfacing Inductor and Ripple Filter for WES	160
5.3.2	Design Principle of SPV-BES System	161
5.4	Control Approaches of SPV-BES-Wind-Based Three-Phase Standalone Microgrids	161

5.4.1	Structure of Developed MSTOGI-MAF Hybrid Algorithm	162
5.4.2	Control of Three-Phase Two-Stage SPV-BES-Wind Based Standalone Microgrid	166
5.4.3	Control of Three-Phase Single-Stage SPV-BES-Wind Based Standalone Microgrid with BDDC	174
5.4.4	Control of Three-Phase Two-Stage SPV-BES-Wind Based Standalone Microgrid with BDDC	175
5.5	MATLAB Based Modelling of SPV-BES-Wind-Based Three-Phase Standalone Microgrids	175
5.6	Hardware Implementation of SPV-BES-Wind-Based Three Phase Standalone Microgrids	177
5.7	Results and Discussion	178
5.7.1	Performance of Three Phase Two-Stage SPV-BES-Wind Based Standalone Microgrid without BDDC	179
5.7.1.1	Simulated Performance of Three-Phase Two-Stage SPV-BES-Wind Based Standalone Microgrid without BDDC	179
5.7.1.2	Experimental Performance of Three-Phase Two-Stage SPV-BES-Wind Based Standalone Microgrid without BDDC	182
5.7.2	Performance of Three-Phase Single-Stage SPV-BES-Wind Based Standalone Microgrid with BDDC	186
5.7.2.1	Simulated Performance of Three-Phase Single-Stage SPV-BES-Wind Based Standalone Microgrid with BDDC	186
5.7.2.2	Experimental Performance of Three-Phase Single-Stage SPV-BES-Wind Based Standalone Microgrid with BDDC	187
5.7.3	Performance of Three-Phase Two-Stage SPV-BES-Wind Based Standalone Microgrid with BDDC	190
5.7.3.1	Simulated Performance of Three-Phase Two-Stage SPV-BES-Wind Based Standalone Microgrid with BDDC	190
5.7.3.2	Experimental Performance of Three-Phase Two-Stage SPV-BES-Wind Based Standalone Microgrid with BDDC	191
5.8	Conclusions	194
<b>CHAPTER-VI CONTROL OF SPV-BES-WIND-DG-BASED THREE-PHASE STANDALONE MICROGRID</b>		<b>196-229</b>
6.1	General	196
6.2	Configurations of SPV-BES-Wind-DG Based Three-Phase Standalone Microgrids	197

6.3	Design of SPV-BES-Wind-DG Based Three-Phase Standalone Microgrids	198
6.4	Control Approaches of SPV-BES-Wind-DG Based Three-Phase Standalone Microgrids	199
6.4.1	Procedure for Operating Modes Selection	200
6.4.2	Relationship Between $X_{DG}$ and $X_{Syn}$ Signals	202
6.4.3	Structure of Developed SOGI- $\alpha\beta$ CDSC-QT1-PLL Algorithm	203
6.4.4	Control of Three-Phase Two-Stage SPV-BES-Wind-DG Based Standalone Microgrids	208
6.4.5	Control of Three-Phase Single-Stage SPV-BES-Wind-DG Based Standalone Microgrids with BDDC	214
6.4.6	Control of Three-Phase Two-Stage SPV-BES-Wind-DG Based Standalone Microgrid with BDDC	214
6.5	MATLAB Based Modelling of SPV-BES-Wind-DG Based Three-Phase Standalone Microgrids	215
6.6	Hardware Implementation of SPV-BES-Wind-DG Based Three-Phase Standalone Microgrids	215
6.7	Results and Discussion	217
6.7.1	Performance of Three-Phase Two-Stage SPV-BES-Wind-DG Based Standalone Microgrid without BDDC	217
6.7.1.1	Simulated Performance of Three-Phase Two-Stage SPV-BES-Wind-DG Based Standalone Microgrid without BDDC	217
6.7.1.2	Real-Time Performance of Three-Phase Two-Stage SPV-BES-Wind-DG Based Standalone Microgrid without BDDC	220
6.7.2	Performance of Three-Phase Single-Stage SPV-BES-Wind-DG Based Standalone Microgrid with BDDC	222
6.7.2.1	Simulated Performance of Three-Phase Single-Stage SPV-BES-Wind-DG Based Standalone Microgrid with BDDC	222
6.7.2.2	Real-Time Performance of Three-Phase Single-Stage SPV-BES-Wind-DG Based Standalone Microgrid with BDDC	224
6.7.3	Performance of Three-Phase Two-Stage SPV-BES-Wind-DG Based Standalone Microgrid with BDDC	224
6.7.3.1	Simulated Performance of Three-Phase Two-Stage SPV-BES-Wind-DG Based Standalone Microgrid with BDDC	226
6.7.3.2	Real-Time Performance of Three-Phase Two-Stage SPV-BES-Wind-DG Based Standalone Microgrid with BDDC	227

6.8	Conclusions	228
<b>CHAPTER-VII CONTROL OF SPV-WIND-BASED THREE-PHASE GRID CONNECTED MICROGRID</b>		<b>230-254</b>
7.1	General	230
7.2	Configurations of SPV-Wind-Based Three-Phase Grid Connected Microgrids	230
7.2.1	Three-Phase Single-Stage SPV-Wind Based Grid Connected Microgrid	231
7.2.2	Three-Phase Two-Stage SPV-Wind Based Grid Connected Microgrid	231
7.3	Design of SPV-Wind-Based Three-Phase Grid Connected Microgrids	232
7.4	Control Approaches of SPV-Wind-Based Three-Phase Grid Connected Microgrids	233
7.4.1	Structure of CLMS Algorithm-Based Harmonics Mitigation and Compensator Method	233
7.4.2	Control of Three-Phase Single-Stage SPV-Wind Based Grid Connected Microgrid	238
7.4.3	Control of Three-Phase Two-Stage SPV-Wind Based Grid Connected Microgrid	242
7.5	MATLAB Based Modelling of SPV-Wind-Based Three-Phase Grid Connected Microgrids	242
7.6	Hardware Implementation of SPV-Wind-Based Three-Phase Grid Connected Microgrids	243
7.7	Results and Discussion	244
7.7.1	Performance of Three-Phase Single-Stage SPV-Wind Based Grid Connected Microgrid	244
7.7.1.1	Simulated Performance of Three-Phase Single-Stage SPV-Wind Based Grid Connected Microgrid	245
7.7.1.2	Experimental Performance of Three-Phase Single-Stage SPV-Wind Based Grid Connected Microgrid	248
7.7.2	Performance of Three-Phase Two-Stage SPV-Wind Based Grid Connected Microgrid	251
7.7.2.1	Simulated Performance of Three-Phase Two-Stage SPV-Wind Based Grid Connected Microgrid	251
7.7.2.2	Experimental Performance of Three-Phase Two-Stage SPV-Wind Based Grid Connected Microgrid	252
7.8	Conclusions	253

<b>CHAPTER-VIII</b>	<b>CONTROL OF SPV-BES-WIND-BASED THREE-PHASE GRID CONNECTED MICROGRIDS</b>	<b>255-290</b>
8.1	General	255
8.2	Configurations of SPV-BES-Wind-Based Three-Phase Grid Connected Microgrids	255
8.3	Design of SPV-BES-Wind-Based Three-Phase Grid Connected Microgrids	256
8.4	Control Approaches of SPV-BES-Wind-Based Three-Phase Grid Connected Microgrids	257
8.4.1	Structure of Designed NFOGI Prefilter-Based PLL	259
8.4.2	Control of Three-Phase Two-Stage SPV-BES-Wind Based Grid Connected Microgrid	264
8.4.3	Control of Three-Phase Single-Stage SPV-BES-Wind Based Grid Connected Microgrid with BDDC	270
8.4.4	Control of Three-Phase Two-Stage SPV-BES-Wind Based Grid Connected Microgrid with BDDC	272
8.5	MATLAB Based Modelling of SPV-BES-Wind-Based Three-Phase Grid Connected Microgrids	272
8.6	Hardware Implementation of SPV-BES-Wind-Based Three-Phase Grid Connected Microgrids	274
8.7	Results and Discussion	274
8.7.1	Performance of Three-Phase Two-Stage SPV-BES-Wind Based Grid Connected Microgrid	275
8.7.1.1	Simulated Performance of Three-Phase Two-Stage SPV-BES-Wind Based Grid Connected Microgrid Under Sudden Unbalanced Load Condition	275
8.7.1.2	Simulated Performance of Three-Phase Two-Stage SPV-BES-Wind Based Grid Connected Microgrid During Change in Operational Mode	277
8.7.1.3	Experimental Performance of Three-Phase Two-Stage SPV-BES-Wind Based Grid Connected Microgrid	279
8.7.2	Performance of Three-Phase Single-Stage SPV-BES-Wind Based Grid Connected Microgrid with BDDC	282
8.7.2.1	Simulated Performance of Three-Phase Single-Stage SPV-BES-Wind Based Grid Connected Microgrid	282
8.7.2.2	Experimental Performance of Three-Phase Single-Stage SPV-BES-Wind Based Grid Connected Microgrid	284
8.7.3	Performance of Three-Phase Two-Stage SPV-BES-Wind Based Grid Connected Microgrid with BDDC	286

8.7.3.1	Simulated Performance of Three-Phase Two-Stage SPV-BES-Wind Based Grid Connected Microgrid with BDDC	286
8.7.3.2	Experimental Performance of Three-Phase Two-Stage SPV-BES-Wind Based Grid Connected Microgrid with BDDC	286
8.10	Conclusions	289
<b>CHAPTER-IX</b>	<b>CONTROL OF MULTIPLE SPV AND WIND-BES DISTRIBUTED GENERATION-BASED THREE-PHASE AC MICROGRID WITH SYNCHRONIZATION</b>	<b>291-310</b>
9.1	General	291
9.2	Configuration of Multiple SPV and Wind-BES Distributed Generation-Based Three-Phase AC Microgrid	291
9.3	Design Of Multiple SPV and Wind-BES Distributed Generation-Based Three-Phase AC Microgrid	292
9.4	Control Approach of Multiple SPV and Wind-BES Distributed Generation-Based Three-Phase AC Microgrid	292
9.4.1	Structure of TOGI-L-SOGI PLL Algorithm	293
9.4.1.1	Analysis of TOGI-L-SOGI-PLL Algorithm and Performance Comparison with Its Counterparts	296
9.4.2	Control Structure of Rooftop SPVS	298
9.4.3	Control Structure of Wind-BES System	300
9.5	MATLAB Based Modelling of Multiple SPV and Wind-BES Distributed Generation-Based Three-Phase AC Microgrid	302
9.6	Hardware Implementation of Multiple SPV and Wind-BES Distributed Generation-Based Three-Phase AC Microgrid	302
9.7	Results and Discussion	302
9.7.1	Simulated Performance of Multiple SPV and Wind-BES Distributed Generation-Based Three-Phase AC Microgrid	303
9.7.1.1	Description of Recorded Results under Changes in Operation Mode of Microgrid from Standalone to Grid-Tied Due to Recovery of AC Grid Supply	303
9.7.1.2	Description of Recorded Results under Sudden Alteration in Control Structure of VCA Controlled Wind-BES System to CCA During Standalone Operation of Microgrid	305
9.7.1.3	Description of Recorded Results under Abrupt Disconnection of VCA Controlled Wind-BES System from PCC During Standalone Operation of Microgrid	306

9.7.2	Real-Time Performance of Multiple SPV and Wind-BES Distributed Generation-Based Three-Phase AC Microgrid	307
9.8	Conclusions	309
<b>CHAPTER-X</b>	<b>MAIN CONCLUSIONS AND SUGGESTIONS FOR FURTHER WORK</b>	<b>311-318</b>
10.1	General	311
10.2	Main Conclusions	312
10.3	Suggestions for Further Work	317
	<b>REFERENCES</b>	<b>319-331</b>
	<b>LIST OF PUBLICATIONS</b>	<b>332-333</b>
	<b>BIO-DATA</b>	<b>334</b>

## LIST OF FIGURES

- Fig. 3.1 Flow-chart to summarize devised configuration of three phase SPVS.
- Fig. 3.2 Circuit configuration of three-phase single-stage SPVS without BES.
- Fig. 3.3 Circuit configuration of three-phase two-stage SPVS without BES.
- Fig. 3.4 Circuit configuration of three-phase two-stage SPVS with direct integration of BES at DC link.
- Fig. 3.5 Circuit configuration of three-phase single-stage SPVS with integration of BES at DC link by a BDDC.
- Fig. 3.6 Circuit configuration of three-phase two-stage SPVS with integration of BES at DC link by a BDDC.
- Fig. 3.7 Flow chart to illustrate selection procedure for operating modes of SPVS.
- Fig. 3.8 Structure of I-CSOGI algorithm with its modified adaptive FLL loop.
- Fig. 3.9 Frequency plot for (a)  $v_{GI}/v_G$  and (b)  $v_{GqI}/v_G$ .
- Fig. 3.10 Impulse response characteristics of SOGI, MSTOGI, CSOGI, and MSOGI algorithms.
- Fig. 3.11 Frequency condition during synchronization (a) with standard FLL (b) with devised modified adaptive FLL.
- Fig. 3.12 Control of three phase single stage SPVS without BES during grid connected mode.
- Fig. 3.13 Flow chart of incremental and conductance based MPPT method to determine  $V_{MPP}$ .
- Fig. 3.14 Control of three phase single stage SPVS without BES during standalone mode.
- Fig. 3.15 Control of BTC for three phase two stage SPVS without BES based configuration.
- Fig. 3.16 Control of PGSC for three phase two stage SPVS with direct integration of BES during grid connected operation.
- Fig. 3.17 PMS to optimize standalone operation of three phase two stage SPVS with direct integration of BES.
- Fig. 3.18 Designed framework to decide operating modes of SPV array in three phase two stage SPVS with direct integration of BES.
- Fig. 3.19 Control of BTC for three phase two stage SPVS with direct integration of BES.
- Fig. 3.20 PMS to regulate AC grid power in grid connected operation of three phase single stage SPVS with Integration of BES at DC link by a BDDC.
- Fig. 3.21 Control of PGSC for single-stage SPVS with integration of BES at dc link by a BDDC during grid connected mode.
- Fig. 3.22 Control of BDDC for three phase single-stage SPVS with integration of BES at DC link by a BDDC.
- Fig. 3.23 Control structure of PGSC for three phase two-stage SPVS with integration of BES at DC link by a BDDC during grid connected operation.
- Fig. 3.24 Designed framework to decide operating modes of SPV array in three phase two stage SPVS with integration of BES at DC link by a BDDC.

- Fig. 3.25 Control structure of BTC for three phase two stage SPVS with integration of BES at DC link by a BDDC.
- Fig. 3.26 MATLAB model of three-phase single-stage SPVS without BES.
- Fig. 3.27 MATLAB model of three-phase two-stage SPVS without BES.
- Fig. 3.28 MATLAB model of three-phase two-stage SPVS with direct integration of BES at DC link.
- Fig. 3.29 MATLAB model of three-phase single-stage SPVS with integration of BES at DC link by a BDDC.
- Fig. 3.30 MATLAB model of three-phase two-stage SPVS with integration of BES at DC link by a BDDC.
- Fig. 3.31 Test bench setup for hardware implementation of designed configurations of three-phase SPVS.
- Fig. 3.32 Schematic of DS1103 PPC controller board with its photograph.
- Fig. 3.33 Photograph of LEM-LA55P Hall Effect current sensor and circuit diagram of current sensor board.
- Fig. 3.34 Photograph of LEM LV-25 Hall Effect voltage sensor and circuit diagram of voltage sensor board.
- Fig. 3.35 Photograph of opto-isolation board and its circuit layout.
- Fig. 3.36 Simulated performance of three phase single stage SPVS without BES during grid connected operational mode (a) under load transient and (b) during variation in SPV array generation.
- Fig. 3.37 FFT results of three phase single stage SPVS without BES during grid connected operational mode (a)-(b)  $v_{Gab-i_{Ga}}$ , (c)  $i_{La}$ , and (d)  $i_{PGSCa}$ .
- Fig. 3.38 Simulated performance of three phase single stage SPVS without BES during standalone operational mode (a) under load transient and (b) during variation in SPV array generation.
- Fig. 3.39 Simulated performance of three phase single stage SPVS without BES during change in operational mode (a) from grid connected to standalone (b) from standalone to grid connected.
- Fig. 3.40 Screenshot of programmable DC power supply software for three phase single stage SPVS without BES during grid connected operational mode.
- Fig. 3.41 Steady state performance of three phase single stage SPVS without BES during grid connected operational mode (a) PCC voltages, load currents, and filtered voltages waveforms (b) grid and PGSC currents with their power quality indices.
- Fig. 3.42 Dynamic performance of three phase single stage SPVS without BES during grid connected operational mode (a) under load transient (b) during variable SPV array generation.
- Fig. 3.43 Steady state performance of three phase single stage SPVS without BES during standalone operational mode.
- Fig. 3.44 Screenshot of programmable DC power supply software for three phase single stage SPVS without BES during standalone operational mode.
- Fig. 3.45 Experimental results for three phase single stage SPVS without BES when operation changes from grid connected to standalone.

- Fig. 3.46 Experimental results for three phase single stage SPVS without BES when operation changes from standalone to grid connected.
- Fig. 3.47 Simulated performance of three phase two stage SPVS without BES during grid connected operational mode (a) under load transient and (b) during variation in SPV array generation.
- Fig. 3.48 Simulated performance of three phase two stage SPVS without BES during change in operational mode (a) from grid connected to standalone (b) from standalone to grid connected.
- Fig. 3.49 Experimental performance of three phase two stage SPVS without BES during grid connected operation mode (a) steady state performance (b) dynamic performance.
- Fig. 3.50 Experimental performance of three phase two stage SPVS without BES during standalone operation mode (a) steady state performance (b) dynamic performance.
- Fig. 3.51 Experimental performance of three phase two stage SPVS without BES during change in operational mode from standalone to grid connected.
- Fig. 3.52 Simulated performance of three phase two stage SPVS with direct integration of BES at DC link during grid connected operational mode (a) under load transient and (b) during variation in SPV array generation.
- Fig. 3.53 FFT results of three phase two stage SPVS with direct integration of BES at DC link during grid connected operational mode.
- Fig. 3.54 Simulated performance of three phase two stage SPVS with direct integration of BES at DC link during standalone operational mode.
- Fig. 3.55 Simulated performance of three phase two stage SPVS with direct integration of BES at DC link during change in operational mode from (a) grid connected to standalone (b) standalone to grid connected.
- Fig. 3.56 Experimental steady state performance of three phase two stage SPVS with direct integration of BES at DC link during grid connected operational mode.
- Fig. 3.57 Experimental dynamic performance of three phase two stage SPVS with direct integration of BES at DC link during grid connected operational mode.
- Fig. 3.58 Experimental performance of three phase two stage SPVS with direct integration of BES at DC link during change in operational mode from (a) grid connected to standalone (b) standalone to grid connected.
- Fig. 3.59 Simulated performance of three phase single stage SPVS with integration of BES at DC link by a BDDC during grid connected operational mode under variable load demand.
- Fig. 3.60 Simulated performance of three phase single stage SPVS with integration of BES at DC link by a BDDC during grid connected operational mode under variable SPV array generation.
- Fig. 3.61 Simulated performance of three phase single stage SPVS with integration of BES at DC link by a BDDC during change in operational mode from (a) grid connected to standalone (b) standalone to grid connected.

- Fig. 3.62 Experimental performance of three phase single stage SPVS with integration of BES at DC link by a BDDC during grid connected operation mode under (a) balanced load and (b) unbalanced load with fully charged BES conditions.
- Fig. 3.63 Experimental performance of three phase single stage SPVS with integration of BES at DC link by a BDDC during grid connected operation mode under variation in (a) load and (b) SPV array power with discharged BES conditions.
- Fig. 3.64 Experimental performance of three phase single stage SPVS with integration of BES at DC link by a BDDC during change in operation mode from (a) grid connected to standalone and (b) standalone to grid connected.
- Fig. 3.65 Simulated performance of three phase two stage SPVS with integration of BES at DC link by a BDDC during grid connected operational mode when BES charge capacity is less than its maximum value.
- Fig. 3.66 FFT results of three phase two stage SPVS with Integration of BES at DC Link by a BDDC during grid connected operational mode.
- Fig. 3.67 Simulated performance of three phase two stage SPVS with integration of BES at DC link by a BDDC during grid connected operational mode when BES is fully charged.
- Fig. 3.68 Simulated performance of three phase two stage SPVS with Integration of BES at DC Link by a BDDC during change in operational mode from (a) grid connected to standalone (b) standalone to grid connected.
- Fig. 3.69 Effect of high penetration of SPV array generation on PCC voltage.
- Fig. 3.70 Experimental performance of three phase two stage SPVS with integration of BES at DC link by a BDDC during grid connected operational mode when BES charge capacity is less than its maximum value from (a) DSO results (b) power analyzer results (i)  $P_{PV}$ , (ii)  $P_B$ , (iii)  $P_{PGSC}$ , (iv)  $P_L$ , (v)  $P_G$ , and (vi)  $v_{Gab}-i_{Ga}$ .
- Fig. 3.71 Experimental performance of three phase two stage SPVS with integration of BES at DC link by a BDDC during grid connected operational mode when BES is fully charged (a) DSO results (b) power analyzer results (i)  $v_{Gab}-i_{Ga}$ , (ii)  $v_{Gab}-i_{PGSCa}$ , (iii)  $v_{Gab}-i_{La}$ , (iv)  $P_G$ , (v)  $P_{PGSC}$ , and (vi)  $P_L$ .
- Fig. 4.1 Circuit configuration of three-phase four-wire single-stage SPVS without BES.
- Fig. 4.2 Circuit configuration of three-phase four-wire two-stage SPVS without BES.
- Fig. 4.3 Circuit configuration of three-phase four-wire two-stage SPVS with direct integration of BES at DC link.
- Fig. 4.4 Circuit configuration of three-phase four-wire single-stage SPVS with integration of BES at DC link by a BDDC.
- Fig. 4.5 Circuit configuration of three-phase four-wire two-stage SPVS with integration of BES at DC link by a BDDC.
- Fig. 4.6 Structure F-LMS filter to determine FAC of load currents and  $I_{LL}$ .
- Fig. 4.7 Performance comparison between F-LMS and LMS algorithms.
- Fig. 4.8 Control of three phase four-wire single stage SPV system without BES.
- Fig. 4.9 Control of three phase four-wire two stage SPV system without BES.
- Fig. 4.10 Control of three phase four-wire two stage SPV system with direct integration of BES.

- Fig. 4.11 Control of three phase four-wire single stage SPV system with integration of BES at dc link by a BDDC.
- Fig. 4.12 Control of three phase four-wire two stage SPV system with integration of BES at dc link by a BDDC.
- Fig. 4.13 MATLAB model of three-phase four-wire single-stage SPV system without BES.
- Fig. 4.14 MATLAB model of three-phase four-wire two-stage SPV system without BES.
- Fig. 4.15 MATLAB model of three-phase four-wire two-stage SPV system with direct integration of BES at DC link.
- Fig. 4.16 MATLAB model of three-phase four-wire single-stage SPV system with integration of BES at DC link by a BDDC.
- Fig. 4.17 MATLAB model of three-phase four-wire two-stage SPV system with integration of BES at DC link by a BDDC.
- Fig. 4.18 Test bench setup for hardware implementation of designed configurations of three-phase four-wire SPV system.
- Fig. 4.19 Simulated performance of three phase four-wire single stage SPV system without BES (a) under load transient and (b) during variation in SPV array generation.
- Fig. 4.20 FFT results of three-phase four-wire single stage SPV system without BES during grid connected operational mode (a)-(b)  $v_{Gab}$ - $i_{Ga}$ , (c)  $i_{La}$ , and (d)  $i_{PGSCa}$ .
- Fig. 4.21 Load current, reference AC grid current, sensed AC grid current network current and PGSC current for three phase four-wire single stage SPV system without BES when (a) SPV system provides no compensation and (b) SPV system provides compensation to local load currents.
- Fig. 4.22 MPPT performance of three phase four-wire single stage SPV system without BES at solar irradiation (a) at  $500 \text{ W/m}^2$  solar irradiance (b) at  $1000 \text{ W/m}^2$  solar irradiance.
- Fig. 4.23 Response of three phase four-wire single stage SPV system without BES under balanced load condition. (a) grid voltage-current ( $v_G, i_G$ ), (b) grid power ( $P_G$ ), (c) grid voltage-current phasor, (d) grid voltage-current THD.
- Fig. 4.24 Response of three phase four-wire single stage SPV system without BES under balanced load condition (a) load voltage-current ( $v_G, i_L$ ), (b) load power ( $P_L$ ), (c) load voltage-current phasor, (d) load voltage-current THD.
- Fig. 4.25 Response of three phase four-wire single stage SPV system without BES under balanced load condition (a) VSC voltage-current ( $v_G, i_{PGSC}$ ), (b) PGSC power ( $P_{PGSC}$ ), (c) PGSC voltage-current phasor (d) PGSC voltage-current THD.
- Fig. 4.26 Response of three phase four-wire single stage SPV system without BES under unbalanced load condition. (a) grid voltage-current ( $v_G, i_G$ ), (b) grid power ( $P_G$ ), (c) grid voltage-current phasor, (d) grid voltage-current THD.
- Fig. 4.27 Response of three phase four-wire single stage SPV system without BES under unbalanced load condition (a) load voltage-current ( $v_G, i_L$ ), (b) load power ( $P_L$ ), (c) load voltage-current phasor, (d) load voltage-current THD.

- Fig. 4.28 Response of three phase four-wire single stage SPV system without BES under unbalanced load condition (a) VSC voltage-current ( $v_G, i_{PGSC}$ ), (b) PGSC power ( $P_{PGSC}$ ), (c) PGSC voltage-current phasor (d) PGSC voltage-current THD.
- Fig. 4.29 Simulated performance of three phase four-wire two stage SPV system without BES (a) under load transient and (b) during variation in SPV array generation.
- Fig. 4.30 Response of three phase four-wire single two SPV system without BES at rated load (a) PV array generation and its MPPT performance (b) PGSC power at PCC (c) AC grid power, and (d) load power.
- Fig. 4.31 Phase “a” current waveforms  $i_{Ga}, i_{La}, i_{PGSCa}$  with phase voltage  $v_{Ga}$  for three phase four-wire single two SPV system without BES.
- Fig. 4.32 THD analysis of phase voltage  $v_{Ga}$  and phase “a” currents  $i_{Ga}, i_{La}, i_{PGSCa}$  for three phase four-wire single two SPV system without BES.
- Fig. 4.33 4<sup>th</sup> wire current  $i_{Gn}, i_{Ln},$  and  $i_{PGSCn}$  for three phase four-wire single two SPV system without BES.
- Fig. 4.34 Response of three phase four-wire single two SPV system without BES at reduced load condition (a) PV array generation and its operating point (b) reduced load power, AC grid power, and PGSC power.
- Fig. 4.35 Simulated performance of three-phase four-wire two stage SPV system with direct integration of BES (a) under load transient and (b) during variation in SPV array generation.
- Fig. 4.36 Experimental performance of three-phase four-wire two stage SPV system with direct integration of BES when (a) SPV system provides no compensation (b) SPV system compensates for local load currents.
- Fig. 4.37 Experimental performance of three-phase four-wire two stage SPV system with direct integration of BES under (a) load transient and (b) during variation in SPV array generation.
- Fig. 4.38 Simulated performance of three-phase four-wire single stage SPV system with integration of BES at DC link by a BDDC under (a) load transient and (b) during variation in SPV array generation.
- Fig. 4.39 Experimental performance of three-phase four-wire single stage SPV system with integration of BES at DC link by a BDDC in balanced nonlinear load condition. (a)-(c) AC current waveforms  $v_{Gab}-i_{Ga}, v_{Gab}-i_{PGSCa}, v_{Gab}-i_{La}$ . (d)-(f) power drawn by grid, PGSC and load (g)-(i) THD value of grid voltage ( $v_{Gab}$ ), grid current ( $i_{Ga}$ ), and load current ( $i_{La}$ ). (j)-(l) neutral current of grid ( $i_{Gn}$ ), PGSC ( $i_{PGSCn}$ ), and load ( $i_{Ln}$ ).
- Fig. 4.40 Experimental performance of three-phase four-wire single stage SPV system with integration of BES at DC link by a BDDC in unbalanced nonlinear load condition. (a)-(c) grid voltage and currents  $v_{Gab}-i_{Ga}, v_{Gbc}-i_{Gb}, v_{Gca}-i_{Gc}$ , (d)-(f) load currents  $v_{Gab}-i_{La}, v_{Gbc}-i_{Lb}, v_{Gca}-i_{Lc}$ , (g)-(i) PGSC currents  $v_{Gab}-i_{PGSCa}, v_{Gbc}-i_{PGSCb}, v_{Gca}-i_{PGSCc}$ , (j)-(l) THD value of grid voltage ( $v_{Gab}$ ), grid current ( $i_{Ga}$ ), and load current ( $i_{La}$ ), (m)-(o) neutral current of grid ( $i_{Gn}$ ), PGSC ( $i_{PGSCn}$ ), and load ( $i_{Ln}$ ).

- Fig. 4.41 Experimental performance of three-phase four-wire single stage SPV system with integration of BES at DC link by a BDDC under (a) load transient and (b) during variation in SPV array generation.
- Fig. 4.42 Simulated performance of three-phase four-wire two stage SPV system with integration of BES at DC link by a BDDC under (a) load transient and (b) during variation in SPV array generation.
- Fig. 4.43 Experimental performance of three-phase four-wire two stage SPV system with integration of BES at DC link by a BDDC (a) SPV array generation, MPPT efficiency, (b) BES voltage, current and power.
- Fig. 4.44 Experimental performance of three-phase four-wire two stage SPV system with integration of BES at DC link by a BDDC under balanced load condition.
- Fig. 4.45 Experimental performance of three-phase four-wire two stage SPV system with integration of BES at DC link by a BDDC under unbalanced load condition.
- Fig. 4.46 Experimental performance of three-phase four-wire two stage SPV system with integration of BES at DC link by a BDDC under (a) load transient and (b) during variation in SPV array generation.
- Fig. 5.1 Circuit configuration of three-phase two-stage SPV-BES-wind based standalone microgrid.
- Fig. 5.2 Circuit configuration of three-phase single-stage SPV-BES-wind based standalone microgrid with BDDC.
- Fig. 5.3 Circuit configuration of three-phase two-stage SPV-BES-wind based standalone microgrid with BDDC.
- Fig. 5.4 Block diagram structure of devised hybrid MSTOGI-MAF algorithm.
- Fig. 5.5 Frequency response of (a) MSTOGI for  $k=1.414$  and (b) MAF for different values of  $T_w$ .
- Fig. 5.6 Step response of MSTOGI across various values of  $k$ .
- Fig. 5.7 Pole-zero plot of MSTOGI across various values of  $k$ .
- Fig. 5.8 Comparison analysis of proposed algorithm with its counterparts.
- Fig. 5.9 Control of three-phase two-stage SPV-BES-wind based standalone microgrid without BDDC.
- Fig. 5.10 Flow-chart for regulation of SPV array and WG outputs in standalone SPV-BES-wind based microgrid according to set constraints of BES.
- Fig. 5.11 Flow-chart of enhance INC method for regulation of SPV array power output.
- Fig. 5.12 Block diagram of sensorless control of SyRG to estimate  $\theta_{\omega_{gest}}$  and  $\omega_{gest}$ .
- Fig. 5.13 Control block diagram of BDDC for three-phase single-stage SPV-BES-wind based standalone microgrid with BDDC.
- Fig. 5.14 MATLAB model of three-phase two-stage SPV-BES-wind based standalone microgrid without BDDC.
- Fig. 5.15 MATLAB model of three-phase single-stage SPV-BES-wind based standalone microgrid with BDDC.
- Fig. 5.16 MATLAB model of three-phase two-stage SPV-BES-wind based standalone microgrid with BDDC.

- Fig. 5.17 Test bench setup for hardware implementation of designed configurations of SPV-BES-wind-based three-phase standalone microgrids.
- Fig. 5.18 Simulated performance of three phase two-stage SPV-BES-wind based standalone microgrid without BDDC under load transient.
- Fig. 5.19 FFT results of PCC voltage ( $v_{Lab}$ ) and load current ( $i_{La}$ ) for three phase two-stage SPV-BES-wind based standalone microgrid without BDDC.
- Fig. 5.20 Simulated performance of three phase two-stage SPV-BES-wind based standalone microgrid without BDDC under load variable SPV array generation.
- Fig. 5.21 Simulated performance of three phase two-stage SPV-BES-wind based standalone microgrid without BDDC under load variable wind speed.
- Fig. 5.22 Snapshot of programmable DC supply software screen, showing MPPT performance of SPV array.
- Fig. 5.23 Performance of implemented sensorless control for SyRG based WG.
- Fig. 5.24 Power quality analyzer results for three phase two-stage SPV-BES-wind based standalone microgrid without BDDC, when it supplies power to unbalanced local loads.
- Fig. 5.25 DSO results for three phase two-stage SPV-BES-wind based standalone microgrid without BDDC, when it supplies power to unbalanced local loads and  $S_{LFC}$  transits from zero to one.
- Fig. 5.26 Simulated performance of three phase single-stage SPV-BES-wind based standalone microgrid with BDDC under load transient.
- Fig. 5.27 Simulated performance of three phase single-stage SPV-BES-wind based standalone microgrid with BDDC under variable SPV array generation.
- Fig. 5.28 Simulated performance of three phase single-stage SPV-BES-wind based standalone microgrid with BDDC under variable wind speed.
- Fig. 5.29 Experimental performance of three phase single-stage SPV-BES-wind based standalone microgrid with BDDC under load transient.
- Fig. 5.30 Experimental performance of three phase single-stage SPV-BES-wind based standalone microgrid with BDDC under variable SPV array generation.
- Fig. 5.31 Experimental performance of three phase single-stage SPV-BES-wind based standalone microgrid with BDDC under variable wind speed.
- Fig. 5.32 Simulated performance of three phase two-stage SPV-BES-wind based standalone microgrid with BDDC under load transient.
- Fig. 5.33 Simulated performance of three phase two-stage SPV-BES-wind based standalone microgrid with BDDC under variable SPV array generation.
- Fig. 5.34 Simulated performance of three phase two-stage SPV-BES-wind based standalone microgrid with BDDC under variable wind speed.
- Fig. 5.35 Power quality analyzer results for three phase two-stage SPV-BES-wind based standalone microgrid with BDDC, when it supplies power to balanced local loads.
- Fig. 5.36 DSO results for three phase two-stage SPV-BES-wind based standalone microgrid with BDDC, when it supplies power to unbalanced local loads and  $S_{LFC}$  transits from zero to one.

- Fig. 5.37 Experimental performance of three phase two-stage SPV-BES-wind based standalone microgrid with BDDC under load transient.
- Fig. 5.38 Experimental performance of three phase two-stage SPV-BES-wind based standalone microgrid with BDDC under variable generation and load demand.
- Fig. 6.1 Circuit configuration of three-phase two-stage SPV-BES-wind-DG based standalone microgrid.
- Fig. 6.2 Circuit configuration of three-phase single-stage SPV-BES-wind-DG based standalone microgrid with BDDC.
- Fig. 6.3 Circuit configuration of three-phase two-stage SPV-BES-wind-DG based standalone microgrid with BDDC.
- Fig. 6.4 Flow-chart to determine operating mode of three-phase SPV-BES-wind-DG based standalone microgrid.
- Fig. 6.5 Flowchart to depict relationship between  $X_{DG}$  and  $X_{Syn}$  signals.
- Fig. 6.6 Block diagram of SOGI-  $\alpha\beta$ CDSC-QT-1PLL algorithm.
- Fig. 6.7 Frequency response of introduced SOGI- $\alpha\beta$ CDSC ( $m = 4, 8$ ) method and its comparison with full-length CDSC ( $m = 2, 4, 8, 16$ ) method.
- Fig. 6.8 Filtering capability assessment of full-length  $\alpha\beta$ CDSC and introduced SOGI- $\alpha\beta$ CDSC methods.
- Fig. 6.9 Dynamic response comparison under step change of (a) +5 Hz in input signal frequency, and (b) +45° in input signal phase.
- Fig. 6.10 Control structure of BTC for three-phase SPV-BES-wind-DG based standalone microgrid.
- Fig. 6.11 Control structure of MSC for three-phase SPV-BES-wind-DG based standalone microgrid.
- Fig. 6.12 Control structure of PGSC for three-phase SPV-BES-wind-DG based standalone microgrid.
- Fig. 6.13 Control structure of WGSC for three-phase SPV-BES-wind-DG based standalone microgrid.
- Fig. 6.14 Control structure of BDDC for three-phase SPV-BES-wind-DG based standalone microgrid.
- Fig. 6.15 MATLAB model of three-phase two-stage SPV-BES-wind-DG based standalone microgrid.
- Fig. 6.16 MATLAB model of three-phase single-stage SPV-BES-wind-DG based standalone microgrid.
- Fig. 6.17 MATLAB model of three-phase two-stage SPV-BES-wind-DG based standalone microgrid with BDDC.
- Fig. 6.18 Test bench setup for experimental assessment of three-phase SPV-BES-wind-DG based standalone microgrids.
- Fig. 6.19 Simulated performance of three phase two-stage SPV-BES-wind-DG based standalone microgrid during change in operational mode from (a) standalone to DG connected (b) DG connected to standalone.
- Fig. 6.20 FFT results of microgrid (a) load voltage and current in standalone operating mode, (b) DG voltage and current in DG connected mode.

- Fig. 6.21 Experimental performance of three phase two-stage SPV-BES-wind-DG based standalone microgrid during change in operational mode from (a) standalone to DG connected (b) DG connected to standalone.
- Fig. 6.22 Recorded waveforms of SPV array parameters, PGSC's DC link voltage, BES current and WG current in experimental analysis of three phase two-stage SPV-BES-wind-DG based standalone microgrid.
- Fig. 6.23 Recorded %THD values of load voltage, DG voltage, load current, and DG current in experimental analysis of three phase two-stage SPV-BES-wind-DG based standalone microgrid.
- Fig. 6.24 Simulated performance of three phase single-stage SPV-BES-wind-DG based standalone microgrid with BDDC during change in operational mode from (a) standalone to DG connected (b) DG connected to standalone.
- Fig. 6.25 Experimental performance of three phase single-stage SPV-BES-wind-DG based standalone microgrid with BDDC during change in operating mode from (a) standalone to DG connected (b) DG connected to standalone.
- Fig. 6.26 Recorded waveforms of SPV array parameters, PGSC's DC link voltage, BES current and WG current in experimental analysis of three phase single-stage SPV-BES-wind-DG based standalone microgrid with BDDC.
- Fig. 6.27 Simulated performance of three phase two-stage SPV-BES-wind-DG based standalone microgrid with BDDC during change in operational mode from (a) standalone to DG connected (b) DG connected to standalone.
- Fig. 6.28 Experimental performance of three phase two-stage SPV-BES-wind-DG based standalone microgrid with BDDC during change in operating mode from (a) standalone to DG connected (b) DG connected to standalone.
- Fig. 6.29 Recorded waveforms of SPV array parameters, PGSC's DC link voltage, BES current and WG current in experimental analysis of three phase two-stage SPV-BES-wind-DG based standalone microgrid with BDDC.
- Fig. 7.1 Circuit configuration of three-phase single-stage SPV-wind based grid connected microgrid.
- Fig. 7.2 Circuit configuration of three-phase two-stage SPV-wind based grid connected microgrid.
- Fig. 7.3 Block diagram of developed C-LMS algorithm for estimation of  $i_{FAC\_L}$ .
- Fig. 7.4 Frequency and step response of C-LMS filter for different values of  $\alpha$ .
- Fig. 7.5 Response of C-LMS algorithm: (a) internal signals under sudden unbalanced load dynamic, and (b) response under sudden introduction of DC offset into sensed load currents.
- Fig. 7.6 Comparison analysis of C-LMS and CSOGI methods.
- Fig. 7.7 Block diagram of discrete CSOGI algorithm for estimation of  $i_{FAC\_L}$ .
- Fig. 7.8 Comparative analysis between performances of C-LMS LMS, SOGI, and CSOGI methods.
- Fig. 7.9 Control structures of GSCs for three-phase single-stage SPV-wind based grid connected microgrid.

- Fig. 7.10 Control structures of BTC for three-phase two-stage SPV-wind based grid connected microgrid.
- Fig. 7.11 MATLAB model of three-phase single-stage SPV-wind based grid connected microgrid.
- Fig. 7.12 MATLAB model of three-phase two-stage SPV-wind based grid connected microgrid.
- Fig. 7.13 Test bench setup for hardware implementation of designed configurations of SPV-wind-based three-phase grid connected microgrids.
- Fig. 7.14 Simulated performance of three phase single-stage SPV-wind based grid connected microgrid under load transient.
- Fig. 7.15 FFT results of PCC voltage ( $v_{Lab}$ ), grid current ( $i_{Ga}$ ), load current ( $i_{La}$ ), PGSC current ( $i_{PGSCa}$ ), WGSC current ( $i_{WGSCa}$ ) for three-phase single-stage SPV-wind based grid connected microgrid.
- Fig. 7.16 Simulated performance of three-phase single-stage SPV-wind based grid connected microgrid under load variable SPV array generation.
- Fig. 7.17 Simulated performance of three-phase single-stage SPV-wind based grid connected microgrid under load variable wind speed.
- Fig. 7.18 Experimental validation of three-phase single-stage SPV-wind based grid connected microgrid's performance with balanced load (a) without and (b) with load compensation.
- Fig. 7.19 Experimental validation of three-phase single-stage SPV-wind based grid connected microgrid's performance with unbalanced load (a) without and (b) with load compensation.
- Fig. 7.20 Simulated performance of three-phase two-stage SPV-wind based grid connected microgrid under load transient.
- Fig. 7.21 Simulated performance of three-phase two-stage SPV-wind based grid connected microgrid under variable SPV array generation.
- Fig. 7.22 Simulated performance of three-phase two-stage SPV-wind based grid connected microgrid under variable wind speed.
- Fig. 7.23 Experimental validation of three-phase two-stage SPV-wind based grid connected microgrid's performance under load transient.
- Fig. 7.24 Experimental validation of three-phase two-stage SPV-wind based grid connected microgrid's performance under under variable generation and load demand.
- Fig. 8.1 Circuit configuration of three-phase two-stage SPV-BES-wind based grid connected microgrid.
- Fig. 8.2 Circuit configuration of three-phase single-stage SPV-BES-wind based grid connected microgrid.
- Fig. 8.3 Circuit configuration of three-phase two-stage SPV-BES-wind based grid connected microgrid with BDDC.
- Fig. 8.4 Structure of NFOGI algorithm.
- Fig. 8.5 Bode and step responses of NFOGI and their comparison with SOGI.

- Fig. 8.6 Algorithms comparison, (a)-(b) Bode diagrams of  $H_I(s)$  and  $Q_I(s)$  and (c)-(d) step responses of  $H_I(s)$  and  $Q_I(s)$ .
- Fig. 8.7 Internal signals of NFOGI algorithm for (a)  $S_\alpha$ , (b)  $S_\beta$ .
- Fig. 8.8 Comparison of NFOGI performance with SOGI, ISOGI, MNG-SOGI algorithms under, (a) balanced three-phase distorted signal, (b) highly unbalanced three-phase distorted signal.
- Fig. 8.9 Control structure of BTC for three-phase SPV-BES-wind-DG based grid connected microgrid.
- Fig. 8.10 Control structure of MSC for three-phase SPV-BES-wind-DG based grid connected microgrid.
- Fig. 8.11 Control structure of PGSC for three-phase SPV-BES-wind-DG based grid connected microgrid.
- Fig. 8.12 Control structure of WGSC for three-phase SPV-BES-wind-DG based grid connected microgrid.
- Fig. 8.13 Structure of designed NFOGI algorithm based HDN to process local load currents.
- Fig. 8.14 Bode diagrams of  $HDN_n(s)$  and  $HDN_{qn}(s)$  for  $n=1$ .
- Fig. 8.15 Control structure of BDDC for three-phase SPV-BES-wind-DG based grid connected microgrid.
- Fig. 8.16 MATLAB model of three-phase two-stage SPV-BES-wind based grid connected microgrid.
- Fig. 8.17 MATLAB model of three-phase single-stage SPV-BES-wind based grid connected microgrid with BDDC.
- Fig. 8.18 MATLAB model of three-phase two-stage SPV-BES-wind based grid connected microgrid with BDDC.
- Fig. 8.19 Test bench setup for hardware implementation of designed configurations of SPV-BES-wind-based three-phase grid connected microgrids.
- Fig. 8.20 Simulated performance of three phase two-stage SPV-BES-wind based grid connected microgrid under sudden unbalanced load condition (a) without regulation of GSCs currents, (b) with regulation of GSCs currents.
- Fig. 8.21 Simulated performance of three phase two-stage SPV-BES-wind based grid connected microgrid during change in operational mode from (a) grid connected to standalone (b) standalone to grid connected.
- Fig. 8.22 Experimental performance of three phase two-stage SPV-BES-wind based grid connected microgrid under, (a) balanced and (b) unbalanced local load condition.
- Fig. 8.23 Experimental performance of three phase two-stage SPV-BES-wind based grid connected microgrid when local load transient from balance to unbalance, (a)-(b) when LCFs of PGSC and WGSC are controlled with formulated control strategy, (c) PGSC and WGSC provide equal LCFs at PCC.
- Fig. 8.24 Simulated performance of three phase single-stage SPV-BES-wind based grid connected microgrid with BDDC during change in operational mode from (a) grid connected to standalone (b) standalone to grid connected.

- Fig. 8.25 Experimental performance of three phase single-stage SPV-BES-wind based grid connected microgrid with BDDC during change in operational mode from (a) grid connected to standalone (b) standalone to grid connected.
- Fig. 8.26 Simulated performance of three phase two-stage SPV-BES-wind based grid connected microgrid with BDDC during change in operational mode from (a) grid connected to standalone (b) standalone to grid connected.
- Fig. 8.27 Experimental performance of three phase two-stage SPV-BES-wind based grid connected microgrid with BDDC during change in operational mode from (a) grid connected to standalone (b) standalone to grid connected.
- Fig. 9.1 Configuration of multiple SPV and wind-BES distributed generation-based three-phase AC microgrid.
- Fig. 9.2 Structure of TOGI-L-SOGI-PLL algorithm.
- Fig. 9.3 Amplitude-phase plot of  $TOGI_p(s)$  and  $TOGI_q(s)$ .
- Fig. 9.4 Amplitude-phase plot of  $L-SOGI(s)$ .
- Fig. 9.5 Internal signals of TOGI-L-SOGI-PLL algorithm.
- Fig. 9.6 Harmonic rejection capability of developed, FOOGI, FIOGI methods.
- Fig. 9.7 Dynamic response under step change in (a) phase angle (b) frequency.
- Fig. 9.8 Control structure of rooftop SPVS.
- Fig. 9.9 Control structure of WGSC of wind-BES system.
- Fig. 9.10 Control structure of BDDC and MSC of wind-BES system.
- Fig. 9.11 MATLAB model of multiple SPV and wind-BES distributed generation-based three-phase AC microgrid.
- Fig. 9.12 Test bench setup for real-time assessment of multiple SPV and wind-BES distributed generation-based three-phase AC microgrid.
- Fig. 9.13 Simulated performance of multiple SPV and wind-BES distributed generation-based three-phase AC microgrid under changes in operation mode of from standalone to grid-tied due to recovery of AC grid supply.
- Fig. 9.14 Simulated performance of multiple SPV and wind-BES distributed generation-based three-phase AC microgrid under sudden alteration in control structure of VCA controlled wind-BES system to CCA during standalone operation of microgrid.
- Fig. 9.15 Simulated performance of multiple SPV and wind-BES distributed generation-based three-phase AC microgrid under abrupt disconnection of VCA controlled wind-BES system from PCC during standalone operation of microgrid.
- Fig. 9.16 Various waveforms of AC grid and wind-BES systems in experimental assessment of multiple SPV and wind-BES distributed generation-based three-phase AC microgrid under changes in operation mode of from standalone to grid-tied due to recovery of AC grid supply.
- Fig. 9.17 Various waveforms of AC grid and rooftop SPVS in experimental assessment of multiple SPV and wind-BES distributed generation-based three-phase AC microgrid under changes in operation mode of from standalone to grid-tied due to recovery of AC grid supply.

- Fig. 9.18 FFT analysis of AC grid voltage and current in experimental assessment of multiple SPV and wind-BES distributed generation-based three-phase AC microgrid during grid-tied operational mode.
- Fig. 9.19 Various waveforms of AC grid and wind-BES systems in experimental assessment of multiple SPV and wind-BES distributed generation-based three-phase AC microgrid under sudden alteration in control structure of VCA controlled wind-BES system to CCA during standalone operation of microgrid.
- Fig. 9.20 Various waveforms of AC grid and rooftop SPVS in experimental assessment of multiple SPV and wind-BES distributed generation-based three-phase AC microgrid under sudden alteration in control structure of VCA controlled wind-BES system to CCA during standalone operation of microgrid.
- Fig. 9.21 FFT analysis of PCC voltage in experimental assessment of multiple SPV and wind-BES distributed generation-based three-phase AC microgrid, when it functions in standalone operational mode.

## LIST OF TABLES

Table 3.1	Design Parameters of Three Phase SPVS
Table 3.2	Harmonic attenuation Capability of SOGI, MSTOGI, CSOGI, and MSOGI Algorithms
Table 3.3	Comparison of SOGI, MSTOGI, CSOGI, and MSOGI Algorithms
Table 4.1	Design Parameters of Three Phase Four-Wire SPV Systems
Table 5.1	Design Parameters of SPV-BES System for Three-Phase SPV-BES-Wind based Standalone Microgrid
Table 5.2	Harmonics Components in Load Currents and its dq Components
Table 5.3	Analysis of MSTOGI-MAF Performance and Comparison with Other Algorithms
Table 5.4	RMS and THD Values of Generated PCC Voltages Before and After Load Transition
Table 6.1	Design Parameters of Three-Phase SPV-BES-Wind-DG based Standalone Microgrid
Table 6.2	Quantitative Comparison of Full-Length CDSC and Introduced Methods
Table 7.1	Design Parameters of Three-Phase SPV-BES-Wind based Grid Connected Microgrid
Table 7.2	Required Mathematical Operators and Computation Burden of C-LMS and CSOGI Methods for Estimating $i_{FAC\_L}$
Table 8.1	Design Parameters of Three-Phase SPV-BES-Wind based Grid Connected Microgrid
Table 8.2	Quantitative Comparison between Algorithms
Table 9.1	Design Parameters of Multiple SPV And Wind-BES Distributed Generation-Based Three-Phase AC Microgrid
Table 9.2	Summary of harmonic Components in $V_G$ and $V_{GI}^+$

## LIST OF ABBREVIATIONS

ADC	Analog-to-Digital Converter
BDDC	Bidirectional DC-DC Converter
BES	Battery Energy Storage
BTC	Boost Converter
CCA	Current Control Algorithm
CDSC	Cascaded Delay Signal Cancellation
C-LMS	Cascaded Least Mean Square
CNF	Complex Notch Filter
CPG	Constant Power Generation
CSOGI	Cascaded Second Order Generalized Integrator
DAC	Digital-to-Analog Converter
DBR	Diode Bridge Rectifier
DFIG	Doubly-Fed Induction Generator
DG	Diesel Generator
DSC	Delay Signal Cancellation
DSO	Digital Signal Oscilloscope
FAC	Fundamental Active Component
FEZ	Fuel Economy Zone
FLL	Frequency-Locked Loop
F-LMS	Fractional Least Mean Square
FSP	Fractional Signal Processing
GSC	Grid Side Converter
HDN	Harmonic Decoupling Network
HPF	High-Pass Filter
I-CSOGI	Improved Cascaded Second Order Generalized Integrator
IGBT	Insulated Gate Bipolar Transistor
INC	Incremental Conductance
ISOGI	Improved Second Order Generalized Integrator
LCFs	Load Compensation Features
LMS	Least Mean Square
L-SOGI	Low-Pass Second Order Generalized Integrator
MAF	Moving Average Filter
MCCF	Multiple Complex Coefficient Filter
MMSE	Minimum Mean Square Error
MNF-SOGI	Modified Notch Filter-based Second Order Generalized Integrator
MNSOGI	Modified Novel Second Order Generalized Integrator
MPP	Maximum Power Point
MPPT	Maximum Power Point Tracking
MSC	Machine Side Converter
MSOGI	Multiple Second Order Generalized Integrator
MSTOGI	Mixed Second and Third-Order Based Generalized Integrator

NFOGI	Novel Fourth-Order Generalized Integrator
NLMS	Normalized Least Mean Square
NSC	Negative Sequence Component
OSG	Orthogonal Signal Generator
PCC	Point of Common Coupling
PCU	Power Conditioner Unit
PEC	Power Electronic Converter
PES	Power Electronics Switches
PI	Proportional Integrator
PGSC	PV Grid Side Converter
PLL	Phase-Locked Loop
PMS	Power Management Scheme
PMSG	Permanent Magnet Synchronous Generator
P&O	Perturb and Observe
PQ	Power Quality
PQA	Power Quality Analyzer
PR	Proportional Resonant
PSC	Positive Sequence Component
PWM	Pulse Width Modulation
QT1-PLL	Quasi-Type-1 Phase-Locked Loop
RES	Renewable Energy Sources
ROGI	Reduce Order Generalized Integrator
SCIG	Squirrel Cage Induction Generator
SD	Steepest Descent
SG	synchronous Generator
SOGI	Second Order Generalized Integrator
SPV	Solar Photovoltaic
SPVS	Solar Photovoltaic System
SRFT	Synchronous Rotating Frame Theory
STS	Static Transfer Switches
SyRG	Synchronous Reluctance Generator
SyRM	Synchronous Reluctance Motor
TOGI	Third-Order Generalized Integrator
UPF	Unity Power Factor
UPS	Uninterruptible Power Supply
UTV	Unit Template Vectors
VCA	Voltage Control Algorithm
VSC	Voltage Source Converter
WES	Wind Energy System
WG	Wind Generator
WGSC	Wind Grid Side Converter
WT	Wind Turbine
WTGA	Wind Turbine Generator Assembly

## LIST OF SYMBOLS

$B_{SOC}$	Charge status of BES.
$B_{SOC\_min}$ and $B_{SOC\_max}$	Set minimum and maximum limits for charge status of BES
$C_{dc1}$ and $C_{dc2}$	DC link capacitor of PGSC and WGSC
$d_{BDDC}$ and $d_{BTC}$	Duty ration of BDDC and BTC
$e_{MPPT}$ , $e_{CPG}$	Estimated error for MPPT and CPG operation of BTC
$f_{DG}$ , $f_G$ , $f_L$	Frequency of DG set voltage, AC grid voltage and PCC voltage
$I_B$ , $V_{BN}$ , $C_B$	Sensed current, nominal voltage, and rated AH capacity of BES
$I_{BR}$	Reference BES current
$I_{Bmax\_C}$ and $I_{Bmax\_D}$	Maximum allowable charging and discharging currents of BES
$\Delta I_B$	Current perturbation used in estimation reference current for BES
$i_{DGa}$ , $i_{DGb}$ , $i_{DGc}$	DG set currents
$i_{DGa}^*$ , $i_{DGb}^*$ , $i_{DGc}^*$	Reference DG set currents
$i_{DGdr}$ , $i_{DGqr}$	dq components of reference DG set currents
$i_{Ga}$ , $i_{Gb}$ , $i_{Gc}$	AC grid currents
$i_{Ga}^*$ , $i_{Gb}^*$ , $i_{Gc}^*$	Reference AC grid currents
$I_{Gn}^*$	Reference current of AC grid neutral wire
$I_{Gd}^*$ , $I_{Gq}^*$	d-q components reference AC grid currents
$i_{La}$ , $i_{Lb}$ , $i_{Lc}$	Local load currents
$i_{La}$ , $i_{L\beta}$	Two-phase or $\alpha\beta$ axis current of local load currents
$i_{La1}^+$ , $i_{Lb1}^+$ , $i_{Lc1}^+$	Filtered PSC of load current
$i_{La1}^+$ , $i_{L\beta1}^+$	Filtered PSC of $\alpha\beta$ axis current of local load currents
$I_{Ld}$ , $I_{Lq}$	d-q components of sensed load current
$I_{Ld1}$ , $I_{Lq1}$	Ripple free d-q components of load current
$i_{FACa}$ , $i_{FACb}$ , and $i_{FACc}$	Amplitudes of fundamental active components of load currents
$I_{LI}$	Average of computed amplitudes of FAC of load currents
$I_{Loss}/I_{Loss1}$	Loss component of PGSC
$I_{Loss2}$	Loss component of WGSC
$i_{PGSCa}$ , $i_{PGSCb}$ , $i_{PGSCc}$	PGSC currents
$I_{SC}$ , $I_{MPP}$ , $I_{PV}$	Short circuit current, MPP current and sensed current of SPV array
$I_{PVref}$	Reference SPV array current
$I_{sw}$ and $V_{sw}$	Current and voltage rating of VSC's switch
$i_{WGSCa}$ , $i_{WGSCb}$ , $i_{WGSCc}$	WGSC currents
$i_{\omega ga}$ , $i_{\omega gb}$ , $i_{\omega gc}$	Wind generator currents
$i_{\omega ga}$ , $i_{\omega \beta}$	$\alpha\beta$ components of stator currents of SyRG based wind generator
$i_{\omega ga}^*$ , $i_{\omega gb}^*$ , $i_{\omega gc}^*$	Reference wind generator currents
$I_{d\omega g}$ , $I_{q\omega g}$	dq components of reference wind generator currents
$i_{Gn}$ , $i_{Ln}$ , $i_{PGSCn}$	Neutral wire or 4 <sup>th</sup> wire currents of AC grid, local load and PGSC
$I_{rr}$	Solar irradiation
$I_{PV\_AC}$ , $I_{WG\_AC}$	AC equivalent current corresponding to power generated by SPV array and WG
$L_f$	Interfacing inductor

$L_{fn}$	Interfacing inductor of PGSC's 4 <sup>th</sup> leg.
$L_{BTC}$ and $L_{BDDC}$	Inductors of BTC and BDDC.
$P_B$ and $P_L$	Estimated powers of BES and local load
$P_{DG}$ and $Q_{DG}$	Estimated active and reactive powers of DG set
$P_G$ and $Q_G$	Estimated active and reactive powers of AC grid
$P_{PV}$ and $P_{WG}$	Estimated powers of SPV array and WG
$P_{GEN}$	Total generated power by SPV array and WG
$P_{WT}$	Generated mechanical power from wind turbine
$P_{Bmax}$	Maximum charging power capacity of BES
$P_{BR}$	Reference power for BES
$P_{GR}, Q_{GR}$	Reference active and reactive powers for AC grid
$P_{G\_max}$	Injected maximum power into AC grid during CPG operation of SPV system
$P_{PVM}$	Signal used to control operation of SPV array in MPPT and off-MPPT modes
$R_f-C_f$	R-C filter
$S_{LCFs}$	Signal to active load compensation features in GSC
$S_{BDDC}, S_{BTC}$	Gating signals of BDDC and BTC
$S_{PGSC}, S_{WGSC}, S_{MSC}$	Gating signals of PGSC, WGSC and MSC
$T_{WT}$	Wind turbine torque
$T_{\omega g}, T_{\omega g est}, T_{\omega g}^*$	Actual, estimated and reference torque of SyRG based WG
$u_{Ga}, u_{Gb}, u_{Gc}$	In-phase per-unit phase voltages or UTV of AC grid phase voltages
$u_{Ga q}, u_{Gb q}, u_{Gc q}$	Quadrature per-unit phase voltages of AC grid phase voltages
$u_{La}, u_{Lb}, u_{Lc}$	In-phase per-unit phase voltages or UTV of PCC phase voltages
$V_{dc}/V_{dc1}, V_{dcref}/V_{dcref1}$	Sensed DC link voltage of PGSC and its corresponding reference
$V_{dc2}, V_{dcref2}$	Sensed DC link voltage of WGSC and its corresponding reference
$v_{DGab}, v_{DGbc}, v_{DGca}$	DG set line voltages
$v_{Gab}, v_{Gbc}, v_{Gca}$	AC grid line voltages
$v_{Ga}, v_{Gb}, v_{Gc}$	AC grid phase voltages
$v_{Ga}, v_{G\beta}$	Two-phase or $\alpha\beta$ axis voltages of AC grid phase voltages
$v_{Ga1}, v_{G\beta1}$	Filtered in phase components of $v_{Ga}, v_{G\beta}$
$v_{Ga q1}, v_{G\beta q1}$	Filtered in quadrature components of $v_{Ga}, v_{G\beta}$
$v_{Ga1}^+, v_{G\beta1}^+$	Filtered PSC of $\alpha\beta$ axis voltages of AC grid phase voltages
$v_{Lab}, v_{Lbc}, v_{Lca}$	PCC line voltages
$v_{La}, v_{Lb}, v_{Lc}$	PCC phase voltages
$v_{La}, v_{L\beta}$	Two-phase or $\alpha\beta$ axis voltages of PCC phase voltages
$v_{La1}, v_{L\beta1}$	Filtered in phase components of $v_{La}, v_{L\beta}$
$v_{La q1}, v_{L\beta q1}$	Filtered in quadrature components of $v_{La}, v_{L\beta}$
$v_{La1}^+, v_{L\beta1}^+$	Filtered PSC of $\alpha\beta$ axis voltages of AC grid phase voltages
$v_{La}^*, v_{Lb}^*, v_{Lc}^*$	Reference PCC voltages
$V_{Lm}^*, \theta_L^*$	Amplitude and phase of reference PCC voltages
$V_{L\_syn}$ and $\theta_{L\_syn}$	Amplitude and phase of reference PCC voltages for synchronization
$v_{La}, v_{L\beta}$	Two-phase or $\alpha\beta$ axis voltages of PCC phase voltages

$V_{DGm}, V_{Gm}, V_{Lm}$	Estimated amplitude of phase voltage for DG set, AC grid and PCC
$V_{max}$	Predefined maximum limit for PCC voltage
$V_{oc}, V_{MPP}, V_{PV}$	Open circuit voltage, MPP voltage and sensed voltage of SPV array
$V_{PVref}$	Reference SPV array voltage
$\Delta V_{PVr}$	Voltage perturbation used in estimation of $V_{PVref}$
$V_W$	Wind speed
$v_{\omega\alpha}, v_{\omega\beta}$	$\alpha\beta$ components of stator voltages of SyRG based wind generator
$X_{Syn}$	Synchronization signal
$X_{DG}, X_G$	Signal representing status of DG set and AC grid
$f_{samp}$	Sampling frequency
$\theta_{DG}, \theta_G, \theta_L$	Estimated phase angle of DG set, AC grid and PCC voltages
$\theta_{\omega gest}$	Estimated rotor position of SyRG based wind generator
$K$	Constant for controlling C-rate of BES
$k_{pVdc}/k_{pVdc1}, k_{iVdc}/k_{iVdc1}$	Gains of DC link PI regulator in PGSC control
$k_{pVdc2}, k_{iVdc2}$	Gains of DC link PI regulator in WGSC control
$k_{pr\_PGSC}, k_{ir\_PGSC}$	Gains of PR regulator in PGSC control
$k_{pVPV}, k_{iVPV}$	Gains of PI regulator in BTC control
$k_{pV\_BDDC}, k_{iV\_BDDC}$	Gains of BDDC's outer PI controller loop
$k_{pI\_BDDC}, k_{iI\_BDDC}$	Gains of BDDC's inner PI controller loop
$k_{p\_og}, k_{i\_og}$	Gains of speed PI regulator in MSC control.
$\Delta I_{PGSC\_pp}, \Delta I_{WGSC\_pp}$	Peak to peak ripple in PGSC and WGSC currents
$\alpha_L$	Gain of LMS algorithm.
$\alpha_F, \chi$	Gains of fractional component of F-LMS algorithm
$C_P$ and $C_t$	Power and torque coefficients of wind turbine
$\lambda$ and $\beta$	Tip speed ratio and pitch angle of wind turbine
$c_1, c_2, c_3, c_4, c_5, c_6$	Design constants of wind turbine
$G_{WT}, r_{WT}, \omega_{WT}$	Gear box ration, blade radius and rotational speed of wind turbine
$\omega_g, \omega_{gest}, \omega_{gref}$	Actual, estimated and reference speeds or SyRG-based WG
$\lambda_{opt}, \omega_{gopt}$	Optimum TSR and speed of wind generator for MPPT operation
$L_d, L_q$	Direct and quadrature axis inductances of SyRG-based WG
$r_{og}$	Winding resistance of SyRG-based WF
$T_w$ and $N$	Window length of MAF and delay length
$\Psi_{\omega\alpha}, \Psi_{\omega\beta}$	$\alpha\beta$ components of stator fluxes of SyRG based wind generator
$i_{Lhr}$	Harmonics and negative sequence currents of local load